Isotope shift of the electron affinity of carbon measured by photodetachment microscopy

David Bresteau, Cyril Drag, and Christophe Blondel*

Laboratoire Aimé-Cotton, Centre National de la Recherche Scientifique, Université Paris-Sud, École Normale Supérieure de Cachan, F-91405 Orsay Cedex, France

(Received 21 July 2015; published 14 January 2016)

The electron affinity of carbon is measured on a beam of C^- by photodetachment microscopy, with a precision increased by one order of magnitude with respect to the last measurement. Isotopes 12 and 13 are used in succession, which makes it possible to determine the isotope shift of the electron affinity of carbon. The obtained result, about $-7.3(6)\,m^{-1}$, corroborates recent calculations of this shift. The electron affinities of ^{12}C and ^{13}C are 1 017 970.5(10) and 1 017 963.3(10) m^{-1}, i.e., 1.262 122 6(11) and 1.262 113 6(12) eV, respectively.

DOI: 10.1103/PhysRevA.93.013414

I. INTRODUCTION

Among atomic negative ions, C^- received early attention. In a pioneering photodetachment experiment carried out with a carbon arc lamp, Seman and Branscomb measured its photodetachment cross section for wavelengths between 0.4 and 0.8 μm, gave evidence for the existence of a bound ^2D excited term (see Fig. 1), and found the electron affinity ^eA(C) to be 1.25(3) eV [1]. As soon as 1968, C^-, together with O^- and H^-, was used to illustrate the peculiarity of photoelectron angular distributions in the photodetachment case [2]. The binding energy of the metastable ^2D level was first measured by electric-field detachment [3] and was found to be 37(3) meV before photodetachment gave a slightly more precise value: 33(1) meV [4]. The existence of this excited term in the vicinity of the photodetachment threshold and the challenge of calculating binding energies, photodetachment cross sections, and photoelectron angular distributions of a first-row negative ion have motivated numerous experimental and theoretical studies for the last 50 years [5]. Production of a beam of C^- ions from an organic sample is at the heart of the most sensitive technique for radiocarbon dating [6]. Laser photodetachment mass spectrometry was devised to selectively detect $^{13}C^-$ ions in a low-energy ion beam [7].

As a test for *ab initio* calculations, electron affinities have been regarded as one of the most difficult cases, for they are just a small energy difference between two systems with different numbers of bound electrons, with a spatial extension that can be significantly larger for the negative ion due to the more loosely bound character of its outer shell. Error cancellation cannot be expected to hide imperfections of the model as easily as for internal energy differences of a neutral atom. With regard to this particular difficulty, the accuracy of an electron affinity calculation is already a good test of the description of electron correlations. The isotope shift of an electron affinity, as noted by Carette and Godefroid [8], is doubly sensitive to correlation effects: through the negative ion structure and through the specific mass shift parameter. It can thus be considered a critical benchmark for the description of correlated electron systems.

The present study aims at giving an experimental counterpart to the calculation of the isotope shift of the electron affinity of carbon that was performed in 2011 [8] and a more precise value of ^eA(C). Carbon is a lighter anion than all those that have been submitted, up to now, to photodetachment microscopy [9].

II. ELECTRON AFFINITY OF CARBON

A. Calculations

Calculating the electron affinity of the first-row elements has been considered a privileged test bed for all methods applicable to the calculation of atomic wave functions, with a particular sensitivity to the quality of the description of electron correlations. Table I shows how calculations have improved in precision for half a century. The best results were obtained by coupled-cluster methods [31,32]. Subsequent multiconfiguration Hartree-Fock (MCHF) calculations did not try to compete with these calculations but aimed at calculating isotope shifts, hyperfine structures, and transition probabilities [8]. Predictions for the isotope shift of the electron affinity (^{13}C with respect to ^{12}C) are either -8.7 [33] or $-7.038\,m^{-1}$ [8]. The electron affinity of carbon has since been used as a test for other binding-energy calculations [34].

B. Measurements

Measured values of the electron affinity are given in the second part of Table I. The first experimental determinations of ^eA(C) made use of graphite sublimation [28] and dissociation of CO by e^- bombardment [29]. The first laser measurement, 1.27(1) eV, was actually limited by the imprecision of the electron affinity of oxygen ^eA(O), which was used as a reference [2]. Replacing the 1.465(5) value of the time by the present 1.461 11 eV figure for ^eA(O) [9], one gets a slightly better 1.266(6) eV value.

The last measurement was performed by Scheer *et al.* [30], who found 1 017 967(15) m^{-1}, or 1.262 119(20) eV, i.e., a value significantly smaller than the last but one measurement [4]. The present work confirms the latter value.

III. FINE AND HYPERFINE STRUCTURE

Determination of the electron affinity from the experimental values of detachment thresholds requires accurate knowledge of the internal energies of the initial and final species. This

*christophe.blondel@u-psud.fr

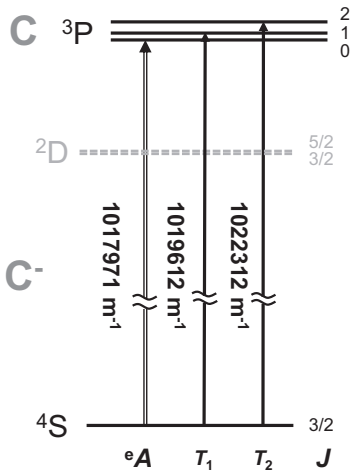

FIG. 1. Level scheme of the C/C$^-$ system, with the electron affinity $^e\!A$ and excited thresholds T_1 and T_2. The bound ^2D doublet of C$^-$ does not play any role in the present study.

raises the question of the fine (FS) and possibly hyperfine (HFS) structure of the C$^-$ anion and C atom, the sublevels of which can provide the initial and final states of the photodetachment process. Fortunately, carbon is a light element and so well known, from a spectroscopic point of view (fine and hyperfine structures are known to a fraction of a megahertz), that the additional uncertainty conveyed by the FS and HFS corrections appears negligible.

A. C$^-$ anion

The $2s^2 2p^3\ ^4S_{3/2}$ ground level of C$^-$ [35] has zero orbital momentum, hence no fine structure, but a unique pure-spin $J = 3/2$ angular momentum.

For the case of $^{13}C^-$ the hyperfine structure has been calculated by Carette and Godefroid [8]. The splitting between the ground $F = 1$ and upper $F = 2$ levels, due to the $I = 1/2$ nuclear spin, is 25.42(25) MHz.

B. Neutral C

1. ^{12}C

The ground level of carbon is the $^3P_0$ level of a $2s^2 2p^2\ ^3P$ triplet [36]. The $^3P_1 - {}^3P_0$ and $^3P_2 - {}^3P_1$ fine-structure intervals were measured to be 492 160.65(6) MHz [37], i.e., 1641.671(1) m^{-1}, and 809 341.97(5) MHz [38], respectively. The energy of the $^3P_2$ level is thus 4341.345(1) m^{-1}. In the present state of our technique, the precision of these fine-structure energy levels is such that measuring the detachment energies to the $^3P_1$ and $^3P_2$ thresholds, one can determine the electron affinity of ^{12}C as precisely as from a direct measurement of the $^3P_0$ threshold.

2. ^{13}C

Due to the $I = 1/2$ spin of the nucleus, the $^3P_1$ and $^3P_2$ levels of ^{13}C are split in two components, as depicted by Fig. 2.

TABLE I. Calculated and measured values (the latter with uncertainty) of the electron affinity of carbon $^e\!A(^{12}C)$. MRCI and MRSD-CI stand for multireference and multireference singles and doubles configuration interaction, respectively. CCSDT stands for coupled-cluster with single, double, and triple excitations, MR-ACPF stands for multireference averaged coupled-pair functional, RHF-DFT stands for relativistic Hartree-Fock density-functional theory, SCSDE stands for self-consistent solution of Dyson's equation, and FCIQMC stands for full configuration-interaction quantum Monte Carlo. As for experimental techniques, PT stands for photodetachment threshold spectroscopy, LPES stands for laser photoelectron spectroscopy, LPT stands for laser phodetachment threshold spectroscopy, and LPM stands for laser photodetachment microscopy.

$^e\!A$ (eV)	Ref.	Year	Method
		Calculations	
1.24	[10]	1960	isoelectronic extrapolation
1.17	[11]	1964	Hartree-Fock with corrections
1.17	[12]	1969	semiempirical
1.29	[13]	1971	orbital Bethe-Goldstone
1.211	[14]	1972	configurational Bethe-Goldstone
1.23	[15]	1974	configuration interaction
1.22	[16]	1985	contracted Gaussian bases
1.22	[17]	1985	Møller-Plesset
1.264	[18]	1991	MRCI
1.245	[19]	1992	MRSD-CI
1.210	[20]	1998	multiconfiguration Dirac-Fock
1.259	[21]	1998	CCSDT
1.193	[22]	1998	Gaussian-3
1.262 3	[23]	1999	MRACPF
1.220	[24]	1999	RHF-DFT
1.262 9	[31]	1999	CCSDT
1.252	[25]	2002	SCSDE
1.262 73	[32]	2010	CCSD
1.269	[26]	2011	i-FCIQMC + ΔE CCSD(T)
1.257 38	[8]	2011	multiconfiguration Hartree-Fock
1.245 44	[27]	2012	MCDHF
		Experiments	
1.2	[28]	1954	graphite sublimation
1.34(19)	[29]	1962	e^- impact on CO
1.25(3)	[1]	1962	PT (unresolved thresholds)
1.266(6)[a]	[2]	1968	LPES @ 488 and 514 nm
1.262 9(3)	[4]	1977	LPT ($^3P_{0,1,2}$ thresholds)
1.262 119(20)	[30]	1998	LPT ($^3P_0$ threshold)
1.262 122 6(11)	this work	2015	LPM ($^3P_{0,1,2}$ thresholds)

[a]Taking an updated value of the electron affinity of oxygen [9] into account. Originally published as 1.27(1) eV.

The performed measurements of the hyperfine components of the $^3P_1 - {}^3P_0$ [37] and $^3P_2 - {}^3P_1$ [38] transitions, together with the measurements of the hyperfine splittings themselves [39,40], can be merged to satisfy the Ritz combination principle [41] and produce an optimized set of hyperfine resolved energy levels. Least-squares fitting here takes an explicit algebraic form [42,43]. This optimization has apparently never been done for the hyperfine-resolved ground term of ^{13}C. The result is given in Table II.

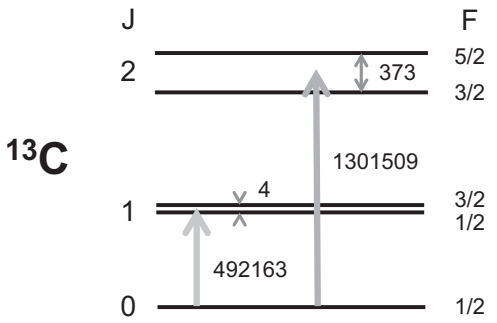

FIG. 2. Hyperfine structure of the ^3P ground term of ^{13}C, with its four independent energy intervals (in MHz). Fine and hyperfine structures are of such different orders of magnitude that the scheme cannot be drawn to scale. The values given for the fine structure are the mean energies of the $^3P_1$ and $^3P_2$ doublets, respectively.

The associated uncertainties can be represented by a covariance matrix Σ (in MHz^2) equal to 10^{-3} times

$$10^3\,\Sigma = \begin{pmatrix} 4.39 & 4.30 & 4.30 & 4.30 \\ 4.30 & 4.82 & 4.79 & 4.79 \\ 4.30 & 4.79 & 12.55 & 11.99 \\ 4.30 & 4.79 & 11.99 & 12.05 \end{pmatrix} \begin{matrix} {}^3P_1\ F=1/2 \\ {}^3P_1\ F=3/2 \\ {}^3P_2\ F=3/2 \\ {}^3P_2\ F=5/2 \end{matrix}.$$

Equivalently, other sets of independent energy intervals can be chosen to describe the hyperfine structure of the ^3P term. A practical one can be composed of the mean energies $^3P_{\bar{1}}$ and $^3P_{\bar{2}}$ of the $J=1$ and $J=2$ doublets and their respective hyperfine splittings $\Delta\nu_1$ and $\Delta\nu_2$, as depicted in Fig. 2. The mean energies $^3P_{\bar{1}}$ and $^3P_{\bar{2}}$, i.e., the weighted averages of the hyperfine energies proportional to their $2F+1$ degeneracy, are the quantities by which the $J=1$ and $J=2$ thresholds appear shifted, with respect to the $J=0$ threshold, in a photodetachment threshold measurement when the resolution is not good enough to distinguish the hyperfine substructure. With this set of energy parameters, as shown by Table III, the greater precision of the $\Delta\nu_1 = {}^3P_1\,3/2 - {}^3P_1\,1/2$ and $\Delta\nu_2 = {}^3P_2\,5/2 - {}^3P_2\,3/2$ hyperfine splittings remains conspicuous, even though merging all data together has substantially reduced the uncertainty of the $^3P_2$ $F=3/2$ and $F=5/2$ energies (which was, e.g., 0.4 MHz for the $F=3/2$ level, if just taken as the uncertainty of one or the other transition leading to this level, in raw data [38]).

TABLE II. Optimized values of the hyperfine sublevels of the ^3P ground term of ^{13}C.

Level	Energy (MHz)	Uncertainty (MHz)
$^3P_1$ $F=1/2$	492 160.136 1	0.066
$^3P_1$ $F=3/2$	492 164.335 4	0.069
$^3P_2$ $F=3/2$	1 301 285.461	0.112
$^3P_2$ $F=5/2$	1 301 658.053	0.110

TABLE III. Optimized values of the mean fine-structure levels of the ^3P ground term of ^{13}C and hyperfine splittings.

Interval	Energy (MHz)	Uncertainty (MHz)
$^3P_{\bar{1}}$	492 162.936	0.067
$\Delta\nu_1$	4.199	0.025
$^3P_{\bar{2}}$	1 301 509.016	0.110
$\Delta\,\nu_2$	372.592	0.025

On this basis, the associated uncertainties are represented by the covariance matrix Σ' equal (in MHz^2) to 10^{-3} times

$$10^3\,\Sigma' = \begin{pmatrix} 4.540 & 0.313 & 4.629 & 0.001 \\ 0.313 & 0.611 & 0.488 & 0.002 \\ 4.629 & 0.488 & 12.101 & -0.190 \\ 0.001 & 0.002 & -0.190 & 0.621 \end{pmatrix} \begin{matrix} {}^3P_{\bar{1}} \\ \Delta\,\nu_1 \\ {}^3P_{\bar{2}} \\ \Delta\,\nu_2 \end{matrix}.$$

The mean $J=1$ and $J=2$ levels have energies of 1641.679(1) and 4341.367(1) m^{-1}, respectively. As shown in the Appendix, the weighting of hyperfine subthresholds is such that the mean fine-structure thresholds are actually the differences between these mean energies and the hyperfine-averaged energy of the initial $^4S_{3/2}$ level. Subtracting the mean $J=1$ and $J=2$ energies from the measured thresholds thus directly gives the mean binding energy of ^{13}C$^-$ $^4S_{3/2}$ states, i.e., the hyperfine-averaged electron affinity. This is the relevant quantity for a comparison with another isotope. The true electron affinity, namely, the binding energy of the $^4S_{3/2}$ $F=1$ ground level of ^{13}C$^-$, is larger by 15.9(2) MHz, i.e., 0.053(1) m^{-1}. It can be directly estimated by subtracting 1641.626(1) and 4341.314(1) m^{-1}, respectively, from the unresolved $^3P_1$ and $^3P_2$ thresholds. In practice, nearly all these hyperfine corrections remain smaller than the resolution of the photodetachment microscope, but the largest splittings may have an influence on the last digit of the measured thresholds.

IV. EXPERIMENTAL SETUP

A. Ion beam and photoelectron collection

The ion beam is produced by a SNICS II cesium sputtering ion source [44], with cathodes made either of pure graphite or of a ^{13}C-enriched compound. In the latter case, composition of the beam was controlled by neutral-atom time-of-flight measurements, following pulsed photodetachment by a frequency-doubled Nd : YAG laser. The beam was found to consist of 94% ^{13}C$^-$ ions.

C$^-$ ions are accelerated from the cathode by a 4.8-kV voltage, then extracted from the ion source by another 2 kV, before being decelerated by 5.6 kV to travel along the ion-beam machine with a 1.2 keV kinetic energy. They are further decelerated by 557 V just before entering the interaction region, down to a 643 eV kinetic energy. For these rather light ions, this corresponds to a velocity of about 10^5 m s^{-1} (depending on the isotope), which may have non-negligible drawbacks in terms of Doppler broadening, but deceleration has to meet a compromise between making the velocity as low as possible and minimizing ion-beam divergence.

In the interaction region, C^- ions are illuminated by a cw Ti : sapphire laser in the presence of a uniform electric field $G = 356\,\mathrm{V\,m^{-1}}$ perpendicular to the ion velocity (in practice, a vertical electric field, produced by parallel horizontal plates). Photodetachment releases some electrons, which are accelerated by the field and imaged by a detector, made of a stack of microchannel plates, a phosphor screen, and a camera, 563 mm off the ion-beam axis. As the accelerated electrons keep the same initial $10^5\,\mathrm{m\,s^{-1}}$ velocity as the ions, parallel to the (horizontal) ion beam, during their whole 134-ns journey to the detector, their detection position appears shifted downstream, (horizontally) in the ion-beam direction, on the detector plane, by about 13 mm. The $4\,\mathrm{km\,s^{-1}}$ difference in velocities between isotopes 12 and 13 results in a separation of the corresponding electrons of more than half a millimeter in the detector plane. Even though the electron distribution on the detector is not a pointlike one (the internal structure of this distribution actually being the object of interest), this 0.5-mm spatial separation contributes to reducing the admixture of the 0.06 times lower $^{12}C^-$ photodetachment signal in the $^{13}C^-$ photoelectron distribution when working with the 13 isotope.

B. Laser

Photodetachment is produced by a cw (Coherent MBR-110) ring Ti : sapphire laser pumped by a frequency-doubled diode-pumped (Coherent Verdi) Nd : YVO_4 laser. The laser wave number, set around 1 018 020, 1 019 670, or 1 022 370 $\mathrm{m^{-1}}$, i.e., typically, $60\,\mathrm{m^{-1}}$ above the $^3P_0$, $^3P_1$, or $^3P_2$ detachment threshold, respectively, is monitored during the whole acquisition sequence and compelled to remain constant within $\pm 0.1\,\mathrm{m^{-1}}$. The wave-number measurement, to this accuracy, is performed with a HighFinesse WS-8 or WS-U lambda meter. Calibration of the lambda meter is repeatedly tested with the light of a diode set to match one of the saturated-absorption hyperfine components of the D2 line of atomic Cs, usually the $6s_{1/2}\,F=4 \rightarrow 6p_{3/2}\,F'=5$ transition at the wave number 1 173 218.18 $\mathrm{m^{-1}}$ [45].

The laser wave numbers for C^- detachment thresholds are on the far IR side of the Ti : sapphire gain curve, which has reduced the available laser power to about 0.2 W. With the smallest wave number and final degeneracy, the $^3P_0$ threshold was especially unfavorable, which was the reason why we did not record photodetachment interferograms for the lowest threshold in ^{13}C.

C. Electron spectrometry

The experiment is carried out using the standard double-spot photodetachment-microscopy setup [46]. With favorable orders of magnitude of both the initial photoelectron energy ϵ and electric field G [47], the observed photoelectron spatial distribution reveals the interference between the half electron wave directly emitted towards the detector and the other half, initially emitted towards higher energies in the electrostatic potential, that is reflected back to the detector by the electric field. Even though the resulting electron distribution can still be called a "spot," it is actually not a simple bell-shaped distribution but an interferogram, with ring-shaped fringes and a maximum action or phase difference $\Delta\Phi$ at the center

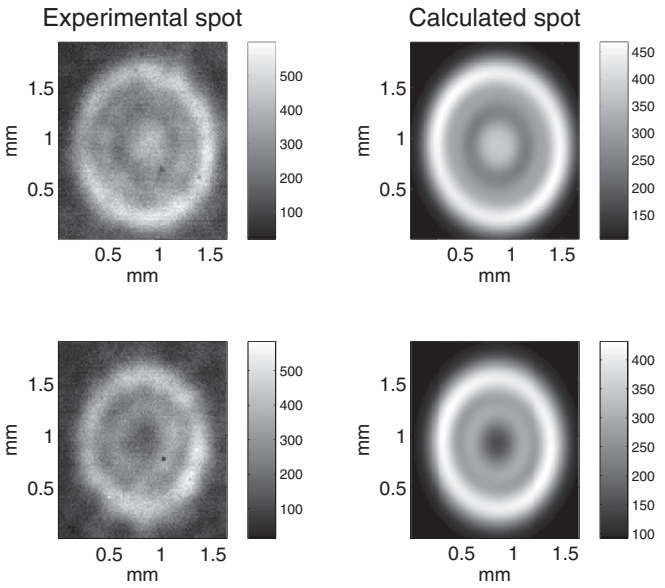

FIG. 3. A pair of experimental photoelectron interferograms (left) obtained by photodetachment of $^{13}C^-$ in an electric field $356\,\mathrm{V\,m^{-1}}$ at a distance of 0.563 m of the electron imaging detector. The laser crosses the C^- ion beam close to right angles, first with a slightly positive Doppler shift (top), then, after reflection, with a slightly negative Doppler shift (bottom). The laser wave number is set at 1 022 366.45 $\mathrm{m^{-1}}$, about $62\,\mathrm{m^{-1}}$ above the $^3P_2$ threshold. The photocurrent (gray scale) is plotted in arbitrary units. The best-fitting synthetic images (right) provide a measurement of the kinetic energy of the photodetached electron: 68.78(50) and 55.97(30) $\mathrm{m^{-1}}$, respectively. Subtracting the half sum $\bar{\epsilon}$ of these two energies from the laser wave number gives a rough estimate of the detachment threshold, 1 022 304 $\mathrm{m^{-1}}$. Corrections are made necessary by the facts that incident and reflected beams are not exactly antiparallel and that the ion beam itself gets deflected by the electric field between the two interaction zones, leading to the actual experimental value of the $^3P_2$ threshold, for this very pair of spots: 1 022 304.55(40) $\mathrm{m^{-1}}$. This is, however, without taking into account the electric field uncertainty, which also affects electron energy measurements carried out by photodetachment microscopy (see text).

of the pattern. Image fitting, when the interference rings are visible, makes it possible to have a very accurate measurement of this phase difference, which is proportional to $\epsilon^{3/2}/G$ [48]. Even though G may be known with only a $\pm 1.5\%$ accuracy and, as a consequence of the previous formula, the relative precision of the ϵ measurement cannot be better than 2/3 of the electric-field relative uncertainty, one can get a measure of the photoelectron energy ϵ with absolute precision orders of magnitude better than that with conventional electron spectrometry, typically $\pm 0.8\,\mathrm{m^{-1}}$, i.e., $\pm 1\,\mu\mathrm{eV}$.

An example of a pair of spots produced by the laser passing forth and back on a $^{13}C^-$ beam is given in Fig. 3. Numerically fitting the electron image with the energy-dependent theoretical interferogram, namely, the Green's function of the uniform acceleration problem [49], we get a measure of the photoelectron kinetic energy for each spot. A slight difference in their numbers of rings $\Delta\Phi/2\pi$ is observed due to a direction-dependent Doppler shift. Combining the energies of the positively and negatively Doppler-shifted spots

into an average value $\bar{\epsilon}$, correcting the photon energy for the second-order Doppler shift, taking into account the facts that the forth and back laser beams are not exactly antiparallel and that the ion beam itself is bent by the electric field between the two interaction zones (typically 3 mm apart), and, of course, knowing the photon energy in the laboratory frame, one can achieve a Doppler-free measurement of the detachment threshold energy [46].

The uncertainty of the photoelectron energy measurement has two main causes. The main one, as just explained, is the uncertainty due to the fact that we only measure $\epsilon^{3/2}/G$ ratios and do not know the value of the applied electric field G better than with $\pm 1.5\%$ precision. The applied electric field, however, is the same for all recordings, which makes it possible to deal with the unknown error of the electric-field value collectively. This will be explained below. The second cause is the specific uncertainty of the numerical procedure that determines, for every experimental spot, the best-fitting synthetic image. The Green's function, which describes electron emission by a pointlike source, cannot actually be used directly as the fitting function and must be convoluted first with experimental response functions to take the finiteness of the spatial and spectral resolutions into account. The widths of these response functions, in both the spatial and spectral domains, may vary and cause additional uncertainties. Granularity of the experiment adds to this uncertainty.

Even though the electric-field uncertainty remains the largest contribution to the photoelectron energy uncertainty, it does not affect the photoelectron energies in uncorrelated ways, which makes some statistical reduction of this uncertainty possible. If all photodetachment events occur in a region of space with about the same electric field, we can expect the relative error due to the electric field to be the same for all measurements. For this reason, the uncertainty due to the electric-field value is not added to the individual error bar of the experimental points but taken into account by a linear regression carried out on every set of data, as for the ones presented in Fig. 4 for the measurements of the $^3P_2$ threshold as a function of the average photoelectron energy $\bar{\epsilon}$. Energies plotted in this figure were calculated assuming that the electric field was exactly 355.9 V m^{-1}. The intercept at zero energy provides us with a threshold measurement made free of any possible bias that would result from a difference between this assumed value and the real one. As a matter of fact, $\bar{\epsilon}$ cannot be varied so much that an accurate determination of the regression slope becomes possible just by looking at the experimental points. But we have a reliable estimate of what the maximum error on the electric-field value G can be. If we can, for example, reliably assume the actual value of the field to be inside a $\pm 1.5\%$ interval with respect to the numerical value used to determine the experimental ϵ values, we can certify that the slope of the regression curve cannot be outside a $\pm 1\%$ interval. In actual calculations, for practical reasons, the linear regression slope is constrained around zero by a normal law, instead of a hat-shaped distribution.

One may also remark that even if the electric field is different from what one has assumed when extracting ϵ values from measured phases, its actual value shall not vary very much from one experiment to the other, as long as one is dealing with the same chemical species. The differences between

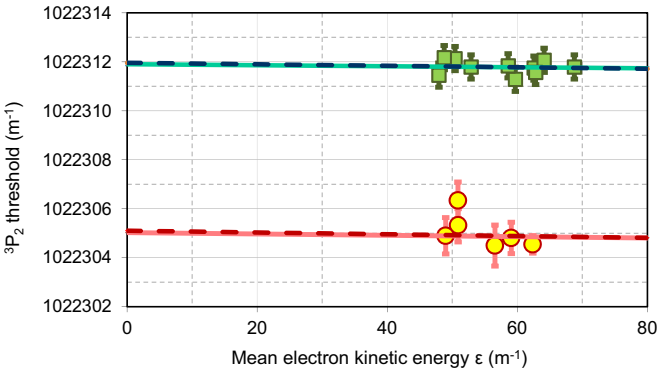

FIG. 4. The isotope shift is made visual in this plot of the apparent $^3P_2$ detachment thresholds of $^{12}C^-$ (squares) and $^{13}C^-$ (circles) as functions of the mean photoelectron kinetic energy. The point that corresponds to the pair of Fig. 3 is the circle with the highest energy, $\bar{\epsilon} = 62.4\,\mathrm{m}^{-1}$. The measured threshold would be constant, as a function of $\bar{\epsilon}$, were it not for a possible error on the electric-field value. Extrapolation down to $\bar{\epsilon} = 0$ produces an error-free measurement. The regression can be made for both shown $^3P_2$ sets of data independently (solid line) or jointly with the similar set of data recorded for the $^3P_1$ and $^3P_0$ thresholds, taking into account the necessary similarity of all five regression slopes (dashed line). The intercept, in the latter case, is 1 022 311.96(95) [1 022 305.11(105)] m^{-1} for isotope 12 (13).

the regression slopes for different detachment thresholds have been constrained, accordingly, around zero with a 0.5% standard deviation or with a 1% standard deviation between different isotopes.

As a matter of fact, the dispersion of the intercept at $\bar{\epsilon} = 0$ keeps the extrapolated threshold uncertainty of the same order of magnitude as the uncertainty of every single measurement. A simple average of the measured thresholds, on a one-dimensional scale, could have produced a more precise result, but with a statistical reduction of the uncertainty which would become illusory for larger samples.

D. Individual threshold measurements

All three photodetachment thresholds of $^{12}C^-$ and both $^3P_1$ and $^3P_2$ photodetachment thresholds of $^{13}C^-$ have been measured using a similar linear regression of the measured values of the apparent threshold down to zero electron kinetic energy. The slope of the linear regression has been constrained, as explained above, around zero with a 1.5% standard deviation. The absolute value of the slope, for the five sets of data taken independently, actually remains well below 1%, ranging from -0.8% to $+0.1\%$. Because essentially the same (unknown) error applies to all experiments carried out with the same ion and, to a lesser extent, to both isotopes, the slope differences have themselves been constrained around zero with standard deviations of 0.5% and 1% for identical and different isotopes, respectively. All slopes, in this case, are brought back to a reduced $[-0.4,-0.3]\%$ interval, with standard deviations even larger than their absolute values. The electric-field error, if the electric-field error is actually to be considered the sole reason for a variation of the apparent threshold with respect to energy, is thus, for the experiments

TABLE IV. Measured photodetachment thresholds. Uncertainties are the sum of twice the statistical standard deviation plus a systematic uncertainty of $\pm 0.13\ \mathrm{m}^{-1}$. Optimized values take the fine-structure measurements and the Ritz combination principle [41] into account.

Threshold	Measured (m^{-1})	Optimized (m^{-1})
	^{12}C	
$^3P_0$	1 017 970.9(13)	1 017 970.5(10)
$^3P_1$	1 019 611.9(11)	1 019 612.2(9)
$^3P_2$	1 022 312.0(10)	1 022 311.9(10)
	^{13}C	
$^3P_{\bar{1}}$	1 019 604.5(11)	1 019 604.9(10)
$^3P_{\bar{2}}$	1 022 305.1(11)	1 022 304.6(10)

carried out on C^-, an especially low one. These are the reasons why the solid (uncoupled) and dashed (coupled) regression lines of Fig. 4 can hardly be distinguished and why these lines appear to be nearly horizontal. Intercept uncertainties, however, remain of the order of $1\ \mathrm{m}^{-1}$.

The measured thresholds are given in Table IV. Uncertainties have been estimated as twice the output standard deviation plus a systematic uncertainty of $\pm 0.13\ \mathrm{m}^{-1}$. The latter is a conservative estimate of the confidence interval of wave-number measurements carried out with a Fizeau WS-8 or WS-U interferometer, as estimated from repeated comparisons of wave-number outputs, initially with an older traveling-cube Michelson interferometer [9], then between different lambda meters of the same kind. Optimized values of the photodetachment thresholds, taking the fine-structure spectroscopy of the neutral atoms into account, are shown in the last column of Table IV. All five measurements are finally merged together to provide the best-fitting electron affinities of both isotopes and the isotope shift. The result is given in Table V.

As for the statistical part, all ^{12}C thresholds have variances and covariances of about $0.14\ \mathrm{m}^{-2}$, all ^{13}C thresholds have variances and covariances of about $0.16\ \mathrm{m}^{-2}$, and 12–13 covariances are all about $0.11\ \mathrm{m}^{-2}$. The identity of variances and covariances, for every isotope, is just due to the fact that fine-structure intervals have been known with precision orders of magnitude better than the precisions we can achieve for the thresholds. The positive covariances between different isotopes reflect the fact that most of the uncertainty, in the present experiment, is due to the uncertainty of the electric-field value, which affects all thresholds in the same way. This positive covariance is especially interesting when estimating unknown threshold differences, such as the isotope shift, the experimental value of which can thus be given with an uncertainty smaller than for separated electron affinities.

TABLE V. Electron affinities of ^{12}C and ^{13}C, with respect to either the hyperfine ground state or a hyperfine averaged ground term, and isotope shift (IS).

	Affinity (m^{-1})	Affinity (eV)
$^eA(^{12}\mathrm{C})$	1 017 970.5(10)	1.262 122 6(11)
$^eA(^{13}\mathrm{C})$	1 017 963.3(10)	1.262 113 6(12)
HF-averaged $^eA(^{13}\mathrm{C})$	1 017 963.2(10)	1.262 113 5(12)
IS $\equiv$ $^eA(^{13}\mathrm{C}) - {}^eA(^{12}\mathrm{C})$	−7.3(6)	$-9(1)\ 10^{-6}$

As predicted, the energy difference between the average $^4S_{3/2}$ level of $^{13}C^-$ and the true $F = 1$ ground level is so small that it only changes the last digit of the electron affinity $^eA(^{13}\mathrm{C})$, depending on whether it is a hyperfine average or the true one. At the indicated precision, no difference appears for the isotope shift.

V. CONCLUSION

The electron affinity of carbon has been measured for the two stable isotopes 12 and 13 and has been found to be 1.262 122 6(11) and 1.262 113 6(12) eV for ^{12}C and ^{13}C, respectively. This is an improvement by a factor of 18, in regard to the precision of the electron affinity of ^{12}C, with respect to the last measurement, which was carried out in 1998 by laser photodetachment threshold spectroscopy [30]. This past and the present measurements appear compatible. The present results confirm that the 1977 measurement [4] was significantly overestimated.

The measured value of the isotope shift, $-7.3(6)\ \mathrm{m}^{-1}$, perfectly matches the $-7.04\ \mathrm{m}^{-1}$ value that has been predicted by theory [8]. This is almost a factor of 2 larger than that with oxygen, the electron affinity of which was found to vary by $-7.4(18)\ \mathrm{m}^{-1}$ from ^{16}O to ^{18}O [50]. Of course the heavier the atom is, the smaller the isotope shift is. There is no surprise in knowing that hydrogen has an especially large isotope shift, with a difference of $320(70)\ \mathrm{m}^{-1}$ between the electron affinities of H and D [51]. In the third row, the normal mass shift of the electron affinity of sulfur was found to be nearly compensated by the specific mass shift, resulting in an especially low shift of $0.23(70)\ \mathrm{m}^{-1}$, from ^{32}S to ^{34}S [52]. The electron affinity isotope shift of chlorine, from ^{35}Cl to ^{37}Cl, is $0.73(47)\ \mathrm{m}^{-1}$, with about two thirds of the normal mass shift still canceled by a negative specific mass shift [53], but the total isotope shift was confirmed to be "definitely normal" by more recent MCHF calculations [54]. The absolute value of the electron affinity isotope shift of bromine, from ^{79}Br to ^{81}Br, was found smaller than $1\ \mathrm{m}^{-1}$ [55]. These are the only measured isotope shifts of electron affinities. An anomalous isotope shift has been predicted for beryllium (which is a special case in the sense that Be^- is a metastable state, formed by attachment of another $2p$ electron to metastable $2s2p$ Be) [56]. Much room is thus left to further investigations, given the interest of these measurements, due to the sensitivity of electron affinities to details of the electronic structure, especially electron correlations.

ACKNOWLEDGMENTS

Thanks are owed to C. Delsart for his continued support, especially in extensive calculations of the hyperfine branching ratios in discrete-to-continuum excitation schemes, and to T. Carette and M. Godefroid, who kindly answered the questions we still had on their electron affinity calculation.

APPENDIX: IDENTITY OF THE HYPERFINE-AVERAGED THRESHOLD AND ENERGY DIFFERENCE BETWEEN HF-AVERAGED LEVELS

Between bound states, it has been known since the early ages of atomic spectroscopy that the mean energy of a transition array is equal to the energy difference between the mean energy levels, averaged independently. This can be inferred, for instance, from Sobel'man's statement that the sum of the intensities of all lines of the hyperfine structure of the transition $\gamma J \to \gamma' J'$ originating from the component F of the level γJ (ending on the component F' of the level $\gamma' J'$) is proportional to the statistical weight of the component $[F]$ ($[F']$) [57]. In the case of photodetachment or photoionization, the algebra is a bit more complicated due to the additional momenta that come into play, as the ejected electron goes away with an individual orbital momentum ℓ and a spin $s = 1/2$.

As already described along with the photodetachment microscopy experiment carried out on P^- [43], the branching ratios towards hyperfine thresholds can be calculated by the fractional parentage method introduced by Engelking and Lineberger [58]. Excitation is described as the "annihilation" of an electron of spin $s = 1/2$ and angular momentum l', which is promoted into the continuum. For the annihilated $2p$ electron of C^-, $l' = 1$, as in all the cases that we have encountered in photodetachment microscopy. The same calculation has already been used to describe the hyperfine structure of the $^{17}O^- \to {}^{17}O$ detachment process [50] for a specific value of the fine-structure quantum numbers, but the hyperfine structure in oxygen, and even more in iodine [59], was large enough to justify that the data analysis be made with an explicit combination of photoelectron images of different energies. For the lighter atom carbon, the hyperfine structure is small enough to make the assumption that the electron interferogram can be fitted in a satisfactory way by the image that corresponds to the mean transition energy. The question is just to check that this mean energy actually corresponds, in principle, to the difference between the mean energies of the final and initial systems.

The relative intensities for s-wave photodetachment, i.e., when the freed electron goes away with an $\ell = 0$ angular momentum, can be expressed as [43]

$$I(J_2,F_2,J_1,F_1) \propto [J_2,F_2,J_1,F_1] \sum_{j'=\ell'-s}^{j'=\ell'+s} [j'] \begin{Bmatrix} F_2 & j' & F_1 \\ J_1 & I & J_2 \end{Bmatrix}^2 \times \begin{Bmatrix} S_1 & L_1 & J_1 \\ s & \ell' & j' \\ S_2 & L_2 & J_2 \end{Bmatrix}^2. \quad \text{(A1)}$$

Summation of the hyperfine components for a given fine-structure threshold means setting the values of the L_1, S_1, J_1 quantum numbers of the initial states of C^- (here no choice: $L_1 = 0, S_1 = 3/2, J_1 = 3/2$), setting the L_2, S_2, J_2 quantum numbers of the final states of C ($L_2 = 1, S_2 = 1, J_2$ can be either 0, 1, or 2), and using the obtained coefficients as weighting factors on a summation of the transition energies $E_2(J_2,F_2) - E_1(J_1,F_1)$ on F_1 and F_2 indices:

$$\overline{E}(J_2,J_1) = \frac{1}{N} \sum_{j'=\ell'-s}^{j'=\ell'+s} [j'] \begin{Bmatrix} S_1 & L_1 & J_1 \\ s & \ell' & j' \\ S_2 & L_2 & J_2 \end{Bmatrix}^2 \times \sum_{F_1,F_2} [J_2,F_2,J_1,F_1] \begin{Bmatrix} F_2 & j' & F_1 \\ J_1 & I & J_2 \end{Bmatrix}^2 \times [E_2(J_2,F_2) - E_1(J_1,F_1)], \quad \text{(A2)}$$

where N is just the normalization factor

$$N = \sum_{F_1,F_2} [J_2,F_2,J_1,F_1] \times \sum_{j'=\ell'-s}^{j'=\ell'+s} [j'] \begin{Bmatrix} F_2 & j' & F_1 \\ J_1 & I & J_2 \end{Bmatrix}^2 \begin{Bmatrix} S_1 & L_1 & J_1 \\ s & \ell' & j' \\ S_2 & L_2 & J_2 \end{Bmatrix}^2. \quad \text{(A3)}$$

The sum over quantum numbers F_1 and F_2 in Eq. (A2) can be separated into two terms, one containing the energy of the final states $E_2(J_2,F_2)$ (with plus signs) and the other the energy of the initial states $E_1(J_1,F_1)$ (with minus signs). The former reads

$$\sum_{F_1,F_2} [J_2,F_2,J_1,F_1] \begin{Bmatrix} F_2 & j' & F_1 \\ J_1 & I & J_2 \end{Bmatrix}^2 E_2(J_2,F_2). \quad \text{(A4)}$$

But 6-j coefficients are normalized so that

$$\sum_{F_1} [J_2,F_1] \begin{Bmatrix} F_2 & j' & F_1 \\ J_1 & I & J_2 \end{Bmatrix}^2 = 1. \quad \text{(A5)}$$

The same applies, symmetrically, to the sum over F_2, which makes it possible to simplify the sum over quantum numbers F_1 and F_2 in Eq. (A2) and write

$$\overline{E}(J_2,J_1) = \frac{1}{N} \sum_{j'=\ell'-s}^{j'=\ell'+s} [j'] \begin{Bmatrix} S_1 & L_1 & J_1 \\ s & \ell' & j' \\ S_2 & L_2 & J_2 \end{Bmatrix}^2 \times \left([J_1] \sum_{F_2} [F_2] E_2(J_2,F_2) - [J_2] \sum_{F_1} [F_1] E_1(J_1,F_1) \right), \quad \text{(A6)}$$

TABLE VI. Weighting matrix for the hyperfine components of the detachment thresholds of ^{13}C, with quantum numbers $L_1 = 0, S_1 = 3/2, J_1 = 3/2$ (initial $^4S_{3/2}$), $I = 1/2, L_2 = 1, S_2 = 1$ (final ^3P), to be divided by a normalization factor 144. One can check that for a fixed J_2 value, vertical sums are in the same ratio as the corresponding $[F_1]$ degeneracies, i.e., like 3 and 5, whereas all horizontal sums are in the same ratios as $[F_2]$ degeneracies.

$^3P_{J_2} \setminus {}^4S_{3/2}$		$F_1 = 1$	$F_1 = 2$
$J_2 = 0$	$F_2 = 1/2$	6	10
$J_2 = 1$	$F_2 = 1/2$	11	5
	$F_2 = 3/2$	7	25
$J_2 = 2$	$F_2 = 3/2$	27	5
	$F_2 = 5/2$	3	45

in which, by construction, the linear combinations of $E_2(J_2, F_2)$, on the one hand, and $E_1(J_1, F_1)$, on the other hand, have been normalized independently. Since the coefficients that appear in these linear combinations are proportional to the degeneracies $[F_2]$ and $[F_1]$, we have exactly here what we looked for:

$$\overline{E}(J_2, J_1) = \overline{E}_2(J_2) - \overline{E}_1(J_1).$$

Numerically, for the case of photodetachment of a $^4S_{3/2}$ negative ion to form a neutral atom in one of the three possible fine-structure states, $^3P_0$,$^3P_1$, or $^3P_2$, the thresholds are weighted by the coefficients given in Table VI.

[1] M. L. Seman and L. M. Branscomb, Phys. Rev. **125**, 1602 (1962).
[2] J. Hall and M. Siegel, J. Chem. Phys. **48**, 943 (1968).
[3] V. Oparin, R. Il'in, I. Serenkov, and E. Solov'ev, Zh. Eksp. Teor. Fiz. **66**, 2008 (1974) [Sov. Phys. JETP **39**, 989 (1974)].
[4] D. Feldmann, Chem. Phys. Lett. **47**, 338 (1977).
[5] T. Andersen, Phys. Rep. **394**, 157 (2004).
[6] M. J. C. Walker, *Quaternary Dating Methods* (Wiley, Chichester, 2005).
[7] P. Andersson, J. Sandström, D. Hanstorp, N. Gibson, K. Wendt, D. Pegg, and R. Thomas, Nucl. Instrum. Methods Phys. Res., Sec. B **266**, 3667 (2008).
[8] T. Carette and M. R. Godefroid, Phys. Rev. A **83**, 062505 (2011).
[9] C. Blondel, W. Chaibi, C. Delsart, C. Drag, F. Goldfarb, and S. Kröger, Eur. Phys. J. D **33**, 335 (2005).
[10] B. Edlén, J. Chem. Phys. **33**, 98 (1960).
[11] E. Clementi and A. McLean, Phys. Rev. **133**, A419 (1964).
[12] İ. Öksüz and O. Sinanoğlu, Phys. Rev. **181**, 54 (1969).
[13] C. Moser and R. Nesbet, Phys. Rev. A **4**, 1336 (1971).
[14] C. Moser and R. Nesbet, Phys. Rev. A **6**, 1710 (1972).
[15] F. Sasaki and M. Yoshimine, Phys. Rev. A **9**, 26 (1974).
[16] D. Feller and E. R. Davidson, J. Chem. Phys. **82**, 4135 (1985).
[17] K. Raghavachari, J. Chem. Phys. **82**, 4142 (1985).
[18] T. Noro, M. Yoshimine, M. Sekiya, and F. Sasaki, Phys. Rev. Lett. **66**, 1157 (1991).
[19] R. A. Kendall, T. H. Dunning, Jr., and R. J. Harrison, J. Chem. Phys. **96**, 6796 (1992).
[20] W. P. Wijesundera and F. A. Parpia, Phys. Rev. A **57**, 3462 (1998).
[21] G. Gutsev, P. Jena, and R. Bartlett, Chem. Phys. Lett. **291**, 547 (1998).
[22] L. A. Curtiss, K. Raghavachari, P. C. Redfern, V. Rassolov, and J. A. Pople, J. Chem. Phys. **109**, 7764 (1998).
[23] R. J. Gdanitz, Chem. Phys. Lett. **312**, 578 (1999).
[24] C. Guo-Xin and P. Ong, J. Phys. B **32**, 5351 (1999).
[25] K. Peirs, D. Van Neck, and M. Waroquier, J. Chem. Phys. **117**, 4095 (2002).
[26] D. Cleland, G. H. Booth, and A. Alavi, J. Chem. Phys. **134**, 024112 (2011).
[27] J. Li, Z. Zhao, M. Andersson, X. Zhang, and C. Chen, J. Phys. B **45**, 165004 (2012).
[28] R. E. Honig, J. Chem. Phys. **22**, 126 (1954).
[29] M. A. Fineman and A. W. Petrocelli, J. Chem. Phys. **36**, 25 (1962).
[30] M. Scheer, R. C. Bilodeau, C. A. Brodie, and H. K. Haugen, Phys. Rev. A **58**, 2844 (1998).
[31] G. de Oliveira, J. M. L. Martin, F. de Proft, and P. Geerlings, Phys. Rev. A **60**, 1034 (1999).
[32] W. Klopper, R. A. Bachorz, D. P. Tew, and C. Hättig, Phys. Rev. A **81**, 022503 (2010).
[33] According to Ref. [8] as per Ref. [32] .
[34] T. Gould and J. F. Dobson, J. Chem. Phys. **138**, 014109 (2013).
[35] T. Andersen, H. K. Haugen, and H. Hotop, J. Phys. Chem. Ref. Data **28**, 1511 (1999).
[36] A. Kramida, Yu. Ralchenko, J. Reader, and NIST ASD Team, NIST Atomic Spectra Database (version 5.2), `http://physics.nist.gov/asd`.
[37] S. Yamamoto and S. Saito, Astrophys. J. Lett. **370**, L103 (1991).
[38] H. Klein, F. Lewen, R. Schieder, J. Stutzki, and G. Winnewisser, Astrophys. J. Lett. **494**, L125 (1998).
[39] G. Wolber, H. Figger, R. Haberstroh, and S. Penselin, Phys. Lett. A **29**, 461 (1969).
[40] G. Wolber, H. Figger, R. Haberstroh, and S. Penselin, Z. Phys. **236**, 337 (1970).
[41] W. Ritz, Astrophys. J. **28**, 237 (1908).
[42] A. Kramida, Comput. Phys. Commun. **182**, 419 (2011).
[43] R. J. Peláez, C. Blondel, M. Vandevraye, C. Delsart, and C. Drag, J. Phys. B **44**, 195009 (2011).
[44] From National Electrostatics Corp.
[45] D. A. Steck, Cesium D Line Data, available online at http://steck.us/alkalidata (revision 2.1.4, 23 December 2010).
[46] C. Blondel, C. Delsart, and F. Goldfarb, J. Phys. B **34**, L281 and erratum 2757 (2001).
[47] C. Blondel, C. Delsart, and F. Dulieu, Phys. Rev. Lett. **77**, 3755 (1996).
[48] C. Blondel, C. Delsart, F. Dulieu, and C. Valli, Eur. Phys. J. D **5**, 207 (1999).
[49] C. Bracher, W. Becker, S. A. Gurvitz, M. Kleber, and M. S. Marinov, Am. J. Phys. **66**, 38 (1998).
[50] C. Blondel, C. Delsart, C. Valli, S. Yiou, M. R. Godefroid, and S. Van Eck, Phys. Rev. A **64**, 052504 (2001).
[51] K. R. Lykke, K. K. Murray, and W. C. Lineberger, Phys. Rev. A **43**, 6104 (1991).
[52] T. Carette, C. Drag, O. Scharf, C. Blondel, C. Delsart, C. Froese Fischer, and M. Godefroid, Phys. Rev. A **81**, 042522 (2010).
[53] U. Berzinsh, M. Gustafsson, D. Hanstorp, A. Klinkmüller, U. Ljungblad, and A.-M. Mårtensson-Pendrill, Phys. Rev. A **51**, 231 (1995).
[54] T. Carette and M. Godefroid, J. Phys. B **46**, 095003 (2013).
[55] C. Blondel, P. Cacciani, C. Delsart, and R. Trainham, Phys. Rev. A **40**, 3698 (1989).
[56] M. Nemouchi, A. Taleb, and M. Godefroid, J. Phys. B **37**, 865 (2004).
[57] I. I. Sobel'man, in *Introduction to the Theory of Atomic Spectra* (Pergamon Press, Oxford, 1972), p. 218.
[58] P. C. Engelking and W. C. Lineberger, Phys. Rev. A **19**, 149 (1979).
[59] R. J. Peláez, C. Blondel, C. Delsart, and C. Drag, J. Phys. B **42**, 125001 (2009).